JCI insight

Treg suppression of immunity within inflamed allogeneic grafts

Hehua Dai, … , Simon c. Watkins, Geoffrey Camirand

JCI Insight. 2022. https://doi.org/10.1172/jci.insight.160579.

Research In-Press Preview Immunology Transplantation

Regulatory $CD4^+Foxp3^+$ T cells (Treg) restrain inflammation and immunity. However, the mechanisms underlying Treg suppressor function in inflamed non-lymphoid tissues remain largely unexplored. Here, we restricted immune responses to non-lymphoid tissues and used intravital microscopy to visualize Treg suppression of rejection by effector T cells (Teff) within inflamed allogeneic islet transplants. Despite their elevated motility, Treg preferentially contact antigen-presenting cells (APCs) over Teff. Interestingly, Treg specifically target APCs that are extensively and simultaneously contacted by Teff. In turn, Treg decrease MHC-II expression on APCs and hinder Teff function. Lastly, we demonstrate that Treg suppressor function within inflamed allografts requires ecto-nucleotidase CD73 activity, which generates the anti-inflammatory adenosine. Consequently, $CD73^{-/-}$ Treg exhibit reduced contacts with APCs within inflamed allografts compared to wt Treg, but not in spleen. Overall, our findings demonstrate that Treg suppress immunity within inflamed grafts through CD73 activity and suggest that Treg-APC direct contacts are central to this process.

Treg suppression of immunity within inflamed allogeneic grafts

Hehua Dai[1], Andressa Pena[1], Lynne Bauer[1], Amanda Williams[1], Simon C. Watkins[2] and Geoffrey Camirand[1]

[1] The Thomas E. Starzl Transplantation Institute, Departments of Surgery and Immunology, University of Pittsburgh School of Medicine, Pittsburgh, PA 15261

[2] Center for Biologic Imaging, Department of Cell Biology and Physiology, University of Pittsburgh School of Medicine, Pittsburgh, PA 15261

Corresponding Author: Geoffrey Camirand, The Thomas E. Starzl Transplantation Institute, University of Pittsburgh School of Medicine, W1543 BST, 200 Lothrop St. Pittsburgh, PA 15261. geoffrey.camirand@pitt.edu

Phone: 412-383-6961 Fax: 412-624-1172

Running Title:

Visualizing Treg suppression within inflamed grafts

SUMMARY

In this study, time-lapse intravital microscopy reveals a central role for antigen-presenting cells and for ecto-nucleotidase CD73 activity in regulatory $CD4^+$ T cell function within inflamed transplanted tissues.

ABSTRACT

Regulatory CD4+$Foxp3^+$ T cells (Treg) restrain inflammation and immunity. However, the mechanisms underlying Treg suppressor function in inflamed non-lymphoid tissues remain largely unexplored. Here, we restricted immune responses to non-lymphoid tissues and used intravital microscopy to visualize Treg suppression of rejection by effector T cells (Teff) within inflamed allogeneic islet transplants. Despite their elevated motility, Treg preferentially contact antigen-presenting cells (APCs) over Teff. Interestingly, Treg specifically target APCs that are extensively and simultaneously contacted by Teff. In turn, Treg decrease MHC-II expression on APCs and hinder Teff function. Lastly, we demonstrate that Treg suppressor function within inflamed allografts requires ecto-nucleotidase CD73 activity, which generates the anti-inflammatory adenosine. Consequently, $CD73^{-/-}$ Treg exhibit reduced contacts with APCs within inflamed allografts compared to wt Treg, but not in spleen. Overall, our findings demonstrate that Treg suppress immunity within inflamed grafts through CD73 activity and suggest that Treg-APC direct contacts are central to this process.

INTRODUCTION

CD4+ Foxp3+ regulatory T cells (Treg) are essential in controlling immunity and inflammation in both secondary lymphoid organs (SLO) and non-lymphoid tissues (1). For example, Treg have been shown to suppress immunity in skin and in tumors (2, 3). In line with this, in transplantation, Treg have been suggested to provide protection from rejection within allogeneic grafts (4-6). In addition to their suppressor function, Treg have been shown to play a role in maintaining homeostasis and promoting tissue repair in peripheral tissues such as visceral adipose tissue, gut mucosa, and skeletal muscle (7, 8). Thus, there is a great interest in harnessing Treg functions for therapeutic purposes in multiple disease settings.

In SLO, Treg can suppress through a multitude of mechanisms (e.g. CTLA-4, IL-10, TGF-β, granzyme B, IL-35, adenosine generation, IL-2 deprivation, inhibition of APCs, and others (9, 10)), suggesting that the mechanisms of suppression by Treg vary according to the local environment. In support of this, Treg were shown to be adaptable to the ongoing T cell effector responses through the expression of concomitant transcription factors (11-14). For example, during a Th1 effector response, which is mediated by the transcription factor T-bet, Treg also differentiate into T-bet$^+$ Th1 regulatory cells. This differentiation enables Treg to migrate to target tissues of effector T cell (Teff) responses by expressing appropriate chemokine receptors and ligands (11). However, the mechanisms underlying Treg suppression in inflamed tissues, specifically in allografts, remains largely unexplored.

To address this, we used a murine model where either graft rejection by Teff or Treg suppression of rejection can only occur within inflamed allogeneic islet transplants. We show that Treg protected from graft rejection by impeding Teff function, without affecting Teff proliferation and accumulation within transplants. Using two-photon intravital microscopy (IVM), we demonstrate that both Teff and Treg accumulate in antigen-presenting cell (APC)-rich areas, and that Treg spend most of their time in contact with APCs. Interestingly, Treg preferentially target APCs that are simultaneously being contacted by Teff. In turn, this leads to a reduction in MHC-II expression

on APCs and to specific inhibition of a subset of Teff that were extensively contacting both APCs and transplanted islets. Lastly, the ecto-nucleotidase CD73 is required for Treg suppressor function within inflamed allografts. Overall, our data demonstrate that Treg counteract inflammation through CD73 activity and suggest that APCs central to Treg suppressor function within inflamed tissues, such as an allograft.

RESULTS

Treg suppress Teff without prior activation in SLO

Although suggested in previous reports (4-6), it remains unclear whether Treg can exert suppressor function within inflamed transplanted tissues. To directly address this, we used an approach that replicates either early rejection by Teff or Treg suppression of rejection by Teff, while restricting the immune responses to transplanted tissues. Allogenic islets were transplanted in diabetic mice lacking all SLO (i.e. splenectomized lymphotoxin β receptor knock-out ($LT\beta R^{-/-}$)). Despite being lymphoreplete, these mice are unable to reject solid allografts unless exogenous effector or memory T cells are transferred (15, 16). To prompt rejection or suppression of rejection, the mice were adoptively transferred with either 2-3x10^6 Teff (containing both $CD4^+$ and $CD8^+$ T cells) alone or with 2-3x10^6 Treg (Fig. 1A). Teff were induced through immunization with donor splenocytes shortly (7 days) prior to adoptive transfer, whereas Treg were harvested from donor-antigen immunized Foxp3 reporter mice after a >30-day rest period post-immunization. As expected (15, 16), splenectomized $LT\beta R^{-/-}$ recipients without cell transfer failed to reject islet allografts, and the transfer of Teff led to acute rejection of islet allografts in all recipients. In contrast, the addition of Treg protected from graft rejection by Teff, delaying rejection initially and providing long-term protection from rejection in ~65% of recipients (Fig. 1B). Interestingly, transferring Treg from naïve mice along with Teff similarly protected from graft rejection (compared to Treg from donor-antigen immunized mice), and this occurred without prior priming of Treg in SLO (Fig. 1B). Comparable results were obtained in another mouse strain lacking SLO (i.e. *aly/aly* mice; Supplemental Fig. 1A-B). These results demonstrate that Treg suppression of Teff can occur in absence of prior priming in SLO.

Treg suppress Teff within the graft directly

We then confirmed that immune responses are restrained to transplanted tissues in our model. Using the same approach as above, but transferring CFSE-labelled congenic T cells, we found that Teff proliferated exclusively within islet allografts (Fig. 1C; top and middle rows; day 3). During

rejection, both $CD4^+$ and $CD8^+$ Teff underwent acute proliferation and extensively accumulated within islet allografts over time (days 3-7; Fig. 1E-F). Treg demonstrated minimal proliferation within allografts compared to Teff (Fig. 1C; bottom row), and showed reduced accumulation rates within allografts over time than Teff (Fig. 1D, third panel) but retained Foxp3 expression (>85%; not shown). Interestingly, despite Treg protection from rejection (Fig. 1B), co-transfer of Treg with Teff had no effect on Teff numbers or proliferation within allografts compared to Teff transferred alone (Fig. 1D-F). In turn, this led to a decrease in Treg:Teff ratios over time (from 12% on day 3 to less than 5% on days 5-7; Fig. 1D, right panel). Taken together, these data demonstrate that our model restricts immune responses to inflamed transplanted tissues, and that both Teff and Treg undergo expansion at that site. While Treg protect from rejection within transplanted tissues, this occurs independently of Teff priming and proliferation at that site. This implies that Treg regulate Teff within the grafted tissue by modulating Teff cytotoxic function.

Teff and Treg are predominantly found in $CD11c^+$ antigen-presenting cells (APC)-rich areas surrounding transplanted islets.

We used IVM to further investigate the mechanisms by which Treg suppress within allografts. The approach described above was modified so that Teff, Treg, $CD11c^+$ APCs, blood vessel lumens and transplanted islets could be imaged simultaneously, using a combination of fluorescent mice and dyes (detailed in Materials and Methods section). In addition, Treg suppression of Teff was optimized (i.e. 100% protection from rejection) by transferring freshly activated Treg (day 7) against donor antigens instead of “rested” Treg (Supplemental Fig. 1C). Given that insulitis (i.e. intra-islet infiltration) is one of the hallmarks of islet destruction by Teff in islet transplantation and in Diabetes (17), we first analyzed large high-resolution 3D intravital images of entire islet grafts on day 4 post-cell transfer. When Teff were transferred alone and rejection was ongoing, only around 20% of Teff were found infiltrating islets (intra-islet) and the large majority (~80%) of Teff were found surrounding the transplanted islets (peri-islet; Fig. 2A, D). Peri-islet infiltration by Teff was especially concentrated in areas rich in $CD11c^+$ APCs (Fig. 2A). Despite this, Teff infiltration

density (i.e. # of Teff / mm^3) in peri-islet vs. intra-islet was not significantly different (Fig. 2F), indicating that there was no preferential accumulation of Teff amongst these areas. In a similar fashion to Teff, $CD11c^+$ APCs distributed predominantly surrounding transplanted islets, but without preferential peri-islet or intra-islet accumulation (Fig. 2A, D-E). The addition of Treg to Teff protected transplanted islets from destruction by Teff (Fig. 2B-C). The large majority of Treg were found in peri-islet areas, where both Teff and $CD11c^+$ APCs were also present (Fig. 2B, D, F). The presence of Treg did not affect Teff and $CD11c^+$ APCs accumulation either peri- or intra-islets (Fig. 2E-F), and the fraction of Treg within transferred T cells were around 20% in all areas (Fig. 2G; as similarly observed by flow cytometry Fig. 1E).

Teff are highly motile during active rejection, making brief and infrequent contacts with $CD11c^+$ APCs and islets.

Time-lapse IVM acquisitions were used to assess graft-infiltrating T cell dynamics and their interactions with one another, with $CD11c^+$ APCs, and with transplanted islets (on day 4 post-cell transfer). As shown in Supplemental Movie 1 and Fig. 3A (top panel), actively rejecting Teff were highly motile and surveyed the entire graft area, while $CD11c^+$ APCs were sessile. Also, occasional dividing Teff were observed (Supplemental Movie 1). Teff contacts with either $CD11c^+$ APCs or islets were relatively brief and infrequent (~2 min each at ~8 contacts/hr; Supplemental Fig. 2A). Only a very small fraction (< 2%) of Teff had prolonged interactions (> 15min) with either $CD11c^+$ APCs or islets (not shown). Consequently, Teff spent around 25% of their time in contact with either $CD11c^+$ APCs or with transplanted islets (Fig. 3C, left panel; contact index: fraction of time spent in contact for each individual cell). Of the small fraction of Teff that had prolonged contacts with islets, this occurred while crawling on the outer surface of the islet tissue (Supplemental Movie 2). Occasionally, some Teff migrated in and out of transplanted islets, demonstrating a previously unappreciated plasticity of Teff dynamics during active rejection (Supplemental Movie 2). Thus, Teff attack transplanted islets from their outer edge, as similarly observed during immune attacks of pancreatic islets in Type I Diabetes (18, 19)

Treg are also highly motile and spend most of their time contacting CD11c$^+$ APCs.

Next, we analyzed the dynamics of Treg within allografts when transferred with Teff. Graft-infiltrating Treg were as motile as Teff, and also surveyed a large fraction of the graft area (Fig. 3A bottom row, 3B, and Supplemental Movie 3) where they made contacts with both CD11c$^+$ APCs and Teff. These contacts were brief (~2 min each) but frequent (12-16 contacts/hr; Supplemental Fig. 2A). Nevertheless, Treg interactions with CD11c$^+$ APCs were significantly longer and more frequent than those with Teff. Thus, despite being quite motile and adjacent to both CD11c$^+$ APCs and Teff, Treg spend most of their time (56%) interacting with CD11c$^+$ APCs than with Teff (37%; Fig. 3C, right panel). In addition, Treg-APC interactions were considerably elevated compared to those of Teff-APC – doubled in their frequency (16 vs. 8 contacts/hr; Supplemental Fig. 2A) and doubled in their contact index (56% vs. 25%; Figure 3C) – demonstrating distinct behaviors between Treg and Teff. These data highlight a possible role for Treg-APC contacts in Treg suppressor function within allografts.

Treg suppress a subset of Teff that preferentially interact with both APCs and islets.

We then assessed how the presence of Treg affected the dynamics of Teff within allografts. Only a small fraction of Teff made direct contact with Treg (less than 20%; not shown) and, on average, Teff only spent around 4% of their time in contact with Treg (Fig. 3A bottom row and 3C). Despite this, the presence of Treg within allografts led to an increase in Teff speed (Fig. 3B). However, Treg did not significantly affect Teff contacts with CD11c$^+$ APCs or with islets, compared to Teff alone (Fig. 3A middle row, 3C and Supplemental Figure 2A). However, we reasoned that Treg may specifically affect subsets of Teff, which would not be reflected in population-wide analyses. To address this, Teff from these IVM datasets were subdivided using unassisted clustering and multi-dimensional t-distributed stochastic neighbor embedding (t-SNE) plots (ViSNE (20)), generated using the IVM-derived parameters listed in Figure 3D. Comparing Teff alone vs. Teff + Treg transfers, we observed a distribution shift in specific Teff subsets that mainly clustered according to their levels of Teff-APC and Teff-islet contacts. Specifically, in the presence of Treg

compared to Teff alone, we observed a 30% frequency increase in Teff that made minimal contacts with both APC and islets (Figure 3D, clusters 1-2 (green and blue)). This was paralleled with a reciprocal 35% frequency decrease in Teff that made substantial contacts with both APC and islets (Figure 3D, clusters 4-5 (black and magenta)). These data further highlight the heterogeneity of Teff behavior within allografts during rejection, and demonstrate that Treg prevent rejection by specifically suppressing a subset of Teff that preferentially contacts both APCs and the target tissue.

Treg preferentially contact CD11c$^+$ APCs that are substantially and simultaneously interacting with Teff.

Given that Treg accumulated in areas rich in both APCs and Teff, we wondered whether Treg contacted CD11c$^+$ APCs that were simultaneously interacting Teff. To address this, we analyzed Teff and Treg contacts made to individual CD11c$^+$ APCs in our IVM datasets where both Teff and Treg were transferred. We compared the fraction of time each individual CD11c$^+$ APC spent in contact with Teff, distinguishing whether APCs were contacted by Teff only, or by both Teff and Treg (Figure 4). We found that around 45% of CD11c$^+$ APCs were contacted by Teff only, around 40% by both Teff and Treg, and around 1% by Treg only (not shown). Interestingly, CD11c$^+$ APCs that were contacted by both Teff and Treg spent more than twice more time in contact with Teff than CD11c$^+$ APCs that were contacted by Teff only (46% vs. 21%; Fig. 4B). Remarkably, the large majority of CD11c$^+$ APC-Treg interactions (64%) occurred while the same APC was simultaneously being contacted by Teff (Fig. 4C, yellow fraction in relation to green fraction). Taken together, these data demonstrate that there is specialization in Treg contacts, where Treg are preferentially attracted towards CD11c$^+$ APCs that are substantially interacting with Teff.

Treg reduce expression of both MHC-II on APCs and IFN-γ in Teff.

Our data demonstrates that Treg within allograft primarily interact with APCs, which correlates with decreased Teff-APC and Teff-islet interactions in a subset of Teff. This suggests that Treg may affect the function of both CD11c$^+$ APCs and Teff. To address this, we first examined whether

Treg affected APC subsets within islet allografts by flow cytometry on day 7 after cell transfer of Teff or Teff + Treg into splenectomized LTβR$^{-/-}$ recipients. We found that nearly all innate cells infiltrating islet allografts expressed CD11c, but with variable levels of CD11b (Supplemental Figure 3A). These CD11c^{+} cells were then clustered into subsets using ViSNE and the parameters listed in Supplemental Figure 3B. Comparing the frequency of the innate cell subsets between transfers of Teff alone and Teff + Treg, we found that the presence of Treg only had moderate effects (Supplemental Figure 3B). Nevertheless, in the presence of Treg, we observed slight decreases in the frequency of innate cell clusters that expressed elevated MHC-II expression (Supplemental Figure 3B, clusters 5-7). In support of this, population-wide analysis of innate cells showed a significant reduction in MHC-II expression levels in the presence of Treg. However, no significant changes were observed in the expression levels of the costimulatory molecules CD80 and CD86 (Figure 5A), as similarly reported by another study investigating the resulting effect of Treg therapy within pancreatic islets (21).

In addition, to assess whether Treg affect Teff function within allografts, we evaluated IFN-γ expression in Teff on day 7. We found that Treg significantly reduced the fraction and absolute numbers of CD4^{+} and CD8^{+} Teff expressing IFN-γ within allografts (Figure. 5B). Taken together, Treg potentially reduce the function of both CD11c^{+} APCs (through a reduction in antigen-presentation) and Teff within allografts.

Intra-graft Treg suppressor function relies on the ecto-nucleotidase CD73

Treg constitutively express the ecto-nucleotidase CD73, which generates anti-inflammatory adenosine from AMP. Adenosine has been shown to inhibit both innate cells and T cells (22-25). Thus, we investigated the role of CD73 in Treg suppressor function within allografts. CD73$^{-/-}$ Treg were equally potent at suppressing T cell proliferation in vitro as wt Treg (Fig. 6A). However, unlike wt Treg, CD73$^{-/-}$ Treg were unable to protect from islet allograft rejection by Teff when transferred in mice lacking SLO (Fig. 6B), demonstrating that CD73 activity on Treg is required for Treg suppression within allografts. We then used IVM to visualize the dynamics and

interactions of Treg with intact suppressor function (wt Treg) vs. Treg with impaired suppressor function ($CD73^{-/-}$ Treg) within inflamed allografts using the same approach as in Figure 3 (day 4). $CD73^{-/-}$ Treg migrated to and accumulated within allografts in comparable fashion to wt Treg, and constituted 29% of the T cell infiltrate on average (not shown). In addition, and similarly to wt Treg, $CD73^{-/-}$ Treg accumulated in peri-islet areas where Teff and $CD11c^{+}$ APCs were also present (Fig. 6C). Despite $CD73^{-/-}$ Treg exhibiting similar motility to wt Treg (Fig. 6D right panel), they made significantly less contacts with $CD11c^{+}$ APCs compared to wt Treg on a population-wide analysis (Fig. 6C, E right panels, and Supplemental Fig. 2B). In support of this, subset clustering of Treg tracks using ViSNE demonstrated a six-fold decrease in $CD73^{-/-}$ Treg making substantial contacts with both APCs and Teff compared to wt Treg (5% vs. 30% respectively; Figure 6F, cluster 3 (green)). This was paralleled with a reciprocal increase in $CD73^{-/-}$ Treg that made minimal contacts with both APCs and Teff (46% for $CD73^{-/-}$ Treg vs. 18% for wt Treg; Figure 6F, cluster 1 (blue)). Interestingly, this altered behavior in $CD73^{-/-}$ vs wt Treg was specific to the inflamed allograft environment, as no significant differences in wt vs. $CD73^{-/-}$ Treg dynamics were observed in steady state spleen (Supplemental Fig. 2C), and $CD73^{-/-}$ mice are not autoimmune (not shown and (26)). We also examined the dynamics of Teff in the presence of $CD73^{-/-}$ Treg. Despite active rejection in these mice, we did not observe significant changes in Teff dynamics compared to Teff co-transferred with wt Treg (Figure 6D-E and Supplemental Figure 2B). Overall, these data demonstrate that CD73 expression is required for Treg suppressor function in inflamed environments, such as an allograft. This impaired suppressor function by $CD73^{-/-}$ Treg is associated with a significant reduction in Treg-APC contacts within allografts, suggesting that these contacts are central in Treg suppressor function. However, the underlying cause(s) of the altered behavior by $CD73^{-/-}$ Treg within allografts remains to be investigated.

DISCUSSION

Our knowledge of the mechanisms underlying Treg suppressor function within inflamed non-lymphoid tissues remains limited, especially in transplanted tissues. Given that Treg adapt to their local environment and the wide variety of mechanisms underlying Treg immunosuppressor function in various tissues (7, 9, 10), uncovering the biology of Treg function in specific conditions has become increasingly important to identify potential therapeutic targets. Here, we demonstrate that Treg do not require prior priming in SLO for their migration and suppression within inflamed allografts. Indeed, circulating Treg readily migrate to inflamed tissues and suppress both APCs and Teff cytotoxic functions. Our IVM data reveal that Treg preferentially interact with APCs that are being significantly contacted by Teff, demonstrating that particular APCs are being targeted by Treg. In turn, Treg suppressor function prevents the generation of Teff with elevated contacts with both APCs and their targets (i.e. transplanted islets). Mechanistically, Treg suppressor function within allografts relies on generating an anti-inflammatory environment through the ecto-nucleotidase CD73. Our data also demonstrate a direct correlation between Treg suppressor function and elevated Treg-APC contacts, as $CD73^{-/-}$ Treg – which are unable to suppress Teff within inflamed allografts – show a drastic reduction in contacts with APCs, compared to wt Treg. A previous IVM publication of transplanted islets placed in the anterior chamber of the eye reported prolonged interactions between Treg and Teff (27), however, this may be caused by the specific microenvironment at that location. In contrast, our report of preferential Treg-APC contact data parallels previous observations in SLO during priming (28-30) and in tumors (31, 32). Biologically, many reasons may explain the requirements and specialization of these Treg-APC contacts. First, APCs provide the required TCR signals for Treg homeostasis, activation and suppressor function (33-36). Thus, Treg-APC interactions in inflamed tissues may be required to provide crucial TCR signals for Treg suppressor function, as previously demonstrated in tumors (31). Second, distinctively functional APCs may secrete T cell-attracting chemokines, which would converge both Treg and Teff to the same APCs. Indeed, recent studies revealed that chemokine

receptor signaling on T cells (CCR5, CXCR3, or CXCR6) promote their interactions with APCs either in SLO or non-SLO (37-39). Similarly, CCR4 or CCR8 signaling in Treg were shown to foster Treg-APC interactions (40, 41). Lastly, Treg-APC interactions may be the result of active suppression of APC function. APCs are targets of Treg suppression, and targeted APCs demonstrate impaired antigenic presentation and reduced capacity to activate conventional T cells through active removal of MHC-II molecules (42), generating soluble tolerogenic factors (43), and/or CTLA-4 mediated suppression (44). Taken together, APCs potentially both promote Treg suppressor function and being the target of Treg suppression. The nature and requirements of these Treg-APC contacts in Treg suppressor function are currently under investigation in our laboratory.

ATP is rapidly released in the extra-cellular space upon tissue injury, which further promotes inflammation through P1 purinergic receptor signaling in immune and parenchymal cells (45). The pro-inflammatory functions of ATP can be reversed by hydrolysis of ATP into adenosine through an enzymatic cascade mediated by CD39 and CD73 extracellular enzymes (46). Adenosine receptor signaling promotes an anti-inflammatory environment through the inhibition of both innate and adaptive immune responses (22-25, 47). Both CD39 and CD73 are constitutively expressed on Treg in mice, and $CD39^{+}$ human Treg demonstrate enhanced suppressor capacity (48, 49). While a previous report attributed a role for adenosine generation in Treg suppressor function in transplantation (25), our data further demonstrate that this Treg suppression mechanism is primarily used within inflamed tissues. In turn, a better understanding of the mechanisms underlying Treg suppressor function within various inflamed tissues will help identifying therapeutic targets that promote such function.

MATERIALS AND METHODS

Animals

Sex-matched 6–10 wk old BALB/c (H-2d), C57BL/6 (B6; H-2b), B6.SJL-*Ptprc*^{a} *Pepc*^{b}/BoyJ (B6.CD45.1; H-2b), B6.Cg-Tg(Itgax-Venus)1Mnz/J (B6.CD11c-YFP), C57BL/6-Foxp3tm1Flv/J (B6.Foxp3-RFP), B6.129S1-Nt5e^{tm1Lft}/J (B6.CD73$^{-/-}$), B6.129(ICR)-Tg(CAG-ECFP)CK6Nagy/J (B6.CFP), C57BL/6-Tg(CAG-EGFP)1Osb/J (B6.eGFP), B6.PL-Thy1^{a}/CyJ (B6.CD90.1) mice from the National Cancer Institute or The Jackson Laboratory were used. B6.Cg-Ltβr^{tm1Mmat}/Rbrc (B6.LTβR$^{-/-}$) were a generous gift from Dr. Mitsuru Matsumoto (50). B6.Foxp3-RFP mice were crossed with B6.CD90.1 in our facility. B6.CD73$^{-/-}$ mice were crossed with B6.Foxp3-RFP.CD90.1 in our facility. In addition, B6.Foxp3-RFP.CD90.1 and B6.Foxp3-RFP.CD90.CD73$^{-/-}$ mice were further crossed with B6.eGFP in our facility. Mice were housed with food and water *ad libitum*.

Islet isolation and Transplantation

Islets from BALB/c donors were digested with Collagenase V or P (Sigma), purified by filtration through a 100-um nylon cell strainer (BD Biosciences), cultured overnight in RMPI-1640 (containing 10% FBS, Penicillin/streptomycin, HEPES, Glutamax, and 2-Mercaptoethanol; Thermo Fisher Scientific), hand-picked under a stereomicroscope, and placed (350-400 islets/recipient) under the left renal capsule of streptozocin-induced (190 mg/kg i.p.; Sigma) diabetic recipients as described (51). For intravital imaging, isolated islets were stained with CellTracker Orange CMRA (10uM for 1hr in RPMI-1640 media; Thermo Fischer Scientific) prior to transplantation. Graft survival was monitored through blood glucose measurements with levels >350 mg/dl over 2 consecutive measurements indicating rejection. Unilateral nephrectomy to remove the transplanted islets was performed to confirm graft function in long-term survivors (>100 days).

Antibodies, Flow Cytometry, and ViSNE analysis

Fluorochrome-conjugated mAbs against CD4 (RM4-5), CD19 (6D5 or 1D3), Foxp3 (FJK-16s), CD45 (30-F11), CD45.1 (A20), CD45.2 (104), CD90.1 (OX-7), CD90.2 (30-H12 or 53-2.1), B220 (RA3-6B2), , NK1.1 (PK136), CD11b (M1/70), CD11c (POD1, HL3, or N418) , Ly6C (HK1.4), Ly6G (1A8), MHC-II (I-A/I-E; M5114.15.2), CD80 (16-10A1), CD86 (GL-1), F4/80 (BM8 or T45-2342), CD16/32 (93), CD8 (53-6.7), IFN-γ (XMG1.2), and Ig control antibodies were from BD Biosciences, Thermo Fisher Scientific, Tonbo Biosciences, or Biolegend. Dead cells were labeled using Fixable Dead Cell Stain (Thermo Fisher Scientific). Negative controls used appropriate Ig fluorochrome conjugates. Flow acquisition was performed on LSRII Fortessa or LSRII analyzers (BD Biosciences). 1-5 x 10^6 events were acquired per sample. Quantitative cell numbers were calculated according to total live cell counts recovered from individual compartments. Tissues were dissociated using 350U/ml Collagenase D (Thermo Fisher Scientific) with 0.02 mg/ml DNAse I (Sigma) in RPMI-1640 media containing 5% FBS at 37C for 30-60 min. under constant agitation. Data were analyzed using FlowJo software (BD Biosciences), and cell doublets and dead cells were excluded from the analysis. For innate cell subset analysis, Lin^+ (i.e. $CD4^+$, $CD8^+$, $NK1.1^+$, $CD19^+$) and $Ly6G^+$ were excluded. For ViSNE analysis, flow cytometry data from live Lin^- $Ly6G^-$ $CD45^+$ $CD11c^+$ singlets were hyperbolic arcsine transformed by a cofactor of 150 before tSNE unsupervised cluster analysis using viSNE in CYT as described (20). For IFN-γ staining, mice received 250 ug Brefeldin A i.p. 4 hours prior to flow cytometry staining as described (52). Digestion of transplanted islets was done with the addition of 10 ug/ml Brefeldin A throughout.

Adoptive cell transfer

Both CD4+ and CD8+ $CD44^{Hi}$ Teff were sort-purified from spleens of B6, B6.CD45.1 or B6.CFP mice immunized with donor splenocytes 5 days prior. Treg were sort-purified from spleens of either naïve B6.Foxp3-RFP.CD90.1 mice; or B6.Foxp3-RFP.CD90.1, B6.Foxp3-RFP.CD90.1.eGFP, B6.Foxp3-RFP.CD90.1.$CD73^{-/-}$, or B6.Foxp3-RFP.CD90.1.$CD73^{-/-}$.eGFP

mice immunized with donor splenocytes 7-30 days prior before cell transfer. 2-3x10^6 Treg and/or Teff were transferred to each recipient 5 days after islet transplantation. In experiments reported in Figure 1 and 5, and Supplemental Figure 1 and 3, Treg were harvested >30 days after immunization with donor splenocytes before cell transfer. In all IVM experiments, Treg were harvested 7 days after immunization with donor splenocytes before cell transfer. In some experiments, Teff and Treg were stained with CFSE (2.0-2.5 μM 5-(and-6)-carboxyfluorescein diacetate, succinimidyl ester; Thermo Fisher Scientific) prior to adoptive transfer.

Two-photon Intravital Microscopy

B6.LTβR$^{-/-}$ mice received total body irradiation (11Gy) using a gamma source and were reconstituted with 5-10x^6 bone marrow cells from B6.CD11c-YFP mice at least 8 weeks before use as islet allograft recipients. Mice were anaesthetized using isoflurane and the kidneys containing the transplanted islets or spleens were surgically exposed and mobilized using custom-made devices four days after cells transfer as we previously described (53, 54). Blood perfusion, mouse rehydration and physiological temperature of 37°C were preserved and maintained throughout the imaging. Two photon laser-scanning imaging was performed using an upright Nikon A1 MP microscope with a Chameleon Ti:Sapphire femtosecond-pulsed laser (Coherent) tuned to 860 nm. Fluorescence emission was captured by four nondescanned GaAsP detectors coupled to the following bandpass emission filters: 480/20, 525/50, 600/60, and 705/55 nm. Time-lapse images were acquired using NIS-Elements software (Nikon). Stacks of 18 optical sections were acquired every 30 seconds for 30 min to provide image volumes of 50 μm (25-55 μm deep) in depth and around 497 μm in width and height at a resolution of 0.994 μm/pixel using a water-immersion 25X objective (NA = 1.1; Nikon).

Two-photon Intravital Microscopy data analysis

Images were spectrally unmixed using NIS-Elements (Nikon). Image rendering, motion artifact correction, surfaces generation, and individual cell tracking of adoptively transferred cells, CD11c+ cells, and of transplanted islets from time-sequence of image stacks was performed

using Imaris software (Bitplane). Cell tracks < 2 min were excluded from analysis. For each dataset, randomly picked tracks were visually inspected to ensure accuracy. Transplanted islet size was evaluated using surface seed splitting size of 75 μm. For contact measurements, voxels inside surfaces were masked with a specific fixed value that varied amongst individual cell type and displayed in individual channels. Surfaces overlap during contact and individual cell tracks were then analyzed for masked fixed values from other cell types over time. From this, contact time and frequency were generated. Contact Index reports the fraction of time an individual cell is in contact with a specific cell type over the length of that entire track. Due to spectral unmixing incompatibilities, IVM of Teff + Treg had to be performed in two separate datasets: one where Treg were non-fluorescent, and another where Treg were fluorescently labeled (eGFP-Treg). In datasets were non-fluorescent Treg were used, Teff tracking parameters and Teff contacts were extracted. In datasets were fluorescent Treg were used, Treg tracking parameters and Treg contacts were extracted. ViSNE was used for multi-parameter IVM tracking analysis. To do so, individual track parameter values were linearly transformed using 1 as maximum, so that each parameter has equal weight in tSNE calculations. Unsupervised cluster analysis and frequency was done using viSNE in CYT. IVM movies were edited using Premier Pro or Photoshop (Adobe).

In Vitro Suppression Assay

Sorted wt or CD73$^{-/-}$ Treg were added to 50k T cells at various ratios in the presence of anti-CD3 and anti-CD28 antibodies in round bottom 96 well plates. After 2 days in culture at 37C, the wells were pulsed with ^{3}H-thymidine and DNA-incorporated thymidine was measured on day 3 using a scintillation beta-counter.

Statistical Analyses

Non-parametric Mann Whitney (comparing two groups), Kruskal-Wallis followed by Dunn's multiple comparison (comparing 3 or more groups), or Logrank Mantel-Cox (for survival curves) tests were used for statistical analyses using Prism (GraphPad). Differences were considered significant at $p < 0.05$. Bars shows mean ± s.e.m, or median as indicated.

Study Approval

Studies were performed in compliance with National Institutes of Health (NIH) guidelines and approved by Institutional Animal Care and Use Committee at the University of Pittsburgh.

Online Supplemental Material

Supplemental Figure 1 (Complement to Fig. 1) shows that Treg can prevent allograft rejection by Teff in a second SLO-deficient mouse model (splenectomized *aly/aly* recipient), and freshly activated Treg provide complete protection from rejection. Supplemental Figure 2 (Complement to Fig. 3 and Fig. 5) shows that Treg contacts with $CD11c^{+}$ APCs are longer and more frequent than those with Teff, and this is lost when Treg lack CD73 expression. Supplemental Figure 3 (Complement to Fig. 4) shows that Treg did not substantially affect the phenotype of innate immune cells infiltrating allografts. Supplemental Figure 4 (Complement to Fig. 5) shows that $CD73^{-/-}$ Treg exhibit similar dynamics to wt Treg in steady state. Supplemental Movie 1 (Complement to Fig. 3) shows time-lapse IVM of islet allograft rejection by Teff. Supplemental Movie 2 (Complement to Fig. 3) shows the dynamics of Teff making prolonged contacts with transplanted islets during rejection. Supplemental Movie 3 (Complement to Fig. 3) shows time-lapse IVM of Treg suppression of islet allograft rejection. Supplemental Movie 4 (Complement to Fig. 3) shows an example of Treg-APC continuous interactions while the same APC simultaneously interacts with Teff.

ACKNOWLEDGMENTS

The authors would like to thank the staff at the Center for Biological Imaging (University of Pittsburgh) and at the Unified Flow Core (University of Pittsburgh) for their tremendous help in many technical aspects. This work was supported by a Young Investigator Award from the National Kidney Foundation (G.C.), by a Scientist Developmental Grant from American Heart Association (16SDG26420129; G.C.), by the Joseph A. Patrick Fellowship at the Starzl Transplantation Institute (G.C.), by the John Merrill Grant in Transplantation from the American Society of Nephrology (G.C.) and by NIAID (U01 AI132758; G.C.). The authors declare no competing financial interests.

AUTHOR CONTRIBUTIONS

H.D., A.P., L.B. and A.W. performed experiments; S.W. provided intellectual contribution and edited the manuscript; and G.C. designed and performed experiments, collected and analyzed data, and wrote the paper.

ABBREVIATIONS

5-(and-6)-carboxyfluorescein diacetate, succinimidyl ester (CFSE); Antigen presenting cells (APCs); Cytotoxic T lymphocyte–associated antigen-4 (CTLA-4); Forkhead box P3 (Foxp3); Interleukin (IL-); Interferon gamma (IFN-γ); Intravital microscopy (IVM); Lymphotoxin β receptor knock-out (LTβR$^{-/-}$); Secondary lymphoid organs (SLO); t-distributed stochastic neighbor embedding (t-SNE); Effector T cells (Teff); Transforming growth factor beta (TGFβ); CD4+ Foxp3+ regulatory T cells (Treg); Wild-type (wt).

REFERENCES

1. Josefowicz SZ, et al. Regulatory T cells: mechanisms of differentiation and function. *Annu Rev Immunol.* 2012;30(1):531-64.
2. Sather BD, et al. Altering the distribution of Foxp3(+) regulatory T cells results in tissue-specific inflammatory disease. *J Exp Med.* 2007;204(6):1335-47.
3. Dadey RE, et al. Regulatory T Cells in the Tumor Microenvironment. *Adv Exp Med Biol.* 2020;1273:105-34.
4. Hu M, et al. Infiltrating Foxp3(+) regulatory T cells from spontaneously tolerant kidney allografts demonstrate donor-specific tolerance. *Am J Transplant.* 2013;13(11):2819-30.
5. Zhang N, et al. Regulatory T cells sequentially migrate from inflamed tissues to draining lymph nodes to suppress the alloimmune response. *Immunity.* 2009;30(3):458-69.
6. Dai Z, et al. CD4+CD25+ regulatory T cells suppress allograft rejection mediated by memory CD8+ T cells via a CD30-dependent mechanism. *J Clin Invest.* 2004;113(2):310-7.
7. Munoz-Rojas AR, and Mathis D. Tissue regulatory T cells: regulatory chameleons. *Nature reviews Immunology.* 2021;21(9):597-611.
8. Panduro M, et al. Tissue Tregs. *Annu Rev Immunol.* 2016;34:609-33.
9. Tang Q, and Bluestone JA. The Foxp3+ regulatory T cell: a jack of all trades, master of regulation. *Nature immunology.* 2008;9(3):239-44.
10. Grover P, et al. Regulatory T Cells: Regulation of Identity and Function. *Front Immunol.* 2021;12:750542.
11. Koch MA, et al. The transcription factor T-bet controls regulatory T cell homeostasis and function during type 1 inflammation. *Nature immunology.* 2009;10(6):595-602.

12. Chaudhry A, et al. CD4+ regulatory T cells control TH17 responses in a Stat3-dependent manner. *Science.* 2009;326(5955):986-91.

13. Zheng Y, et al. Regulatory T-cell suppressor program co-opts transcription factor IRF4 to control T(H)2 responses. *Nature.* 2009;458(7236):351-6.

14. Yang BH, et al. Foxp3(+) T cells expressing RORgammat represent a stable regulatory T-cell effector lineage with enhanced suppressive capacity during intestinal inflammation. *Mucosal Immunol.* 2016;9(2):444-57.

15. Lakkis FG, et al. Immunologic 'ignorance' of vascularized organ transplants in the absence of secondary lymphoid tissue. *Nature medicine.* 2000;6(6):686-8.

16. Chalasani G, et al. Recall and propagation of allospecific memory T cells independent of secondary lymphoid organs. *Proceedings of the National Academy of Sciences of the United States of America.* 2002;99(9):6175-80.

17. In't Veld P. Insulitis in human type 1 diabetes: The quest for an elusive lesion. *Islets.* 2011;3(4):131-8.

18. Coppieters K, et al. Intravital imaging of CTLs killing islet cells in diabetic mice. *J Clin Invest.* 2012;122(1):119-31.

19. Mohan JF, et al. Imaging the emergence and natural progression of spontaneous autoimmune diabetes. *Proceedings of the National Academy of Sciences of the United States of America.* 2017;114(37):E7776-E85.

20. Amir el AD, et al. viSNE enables visualization of high dimensional single-cell data and reveals phenotypic heterogeneity of leukemia. *Nat Biotechnol.* 2013;31(6):545-52.

21. Mahne AE, et al. Therapeutic regulatory T cells subvert effector T cell function in inflamed islets to halt autoimmune diabetes. *Journal of immunology.* 2015;194(7):3147-55.

22. Ohta A, and Sitkovsky M. Role of G-protein-coupled adenosine receptors in downregulation of inflammation and protection from tissue damage. *Nature.* 2001;414(6866):916-20.

23. Sitkovsky MV, et al. Physiological control of immune response and inflammatory tissue damage by hypoxia-inducible factors and adenosine A2A receptors. *Annu Rev Immunol.* 2004;22:657-82.

24. Mandapathil M, et al. Generation and accumulation of immunosuppressive adenosine by human CD4+CD25highFOXP3+ regulatory T cells. *J Biol Chem.* 2010;285(10):7176-86.

25. Deaglio S, et al. Adenosine generation catalyzed by CD39 and CD73 expressed on regulatory T cells mediates immune suppression. *J Exp Med.* 2007;204(6):1257-65.

26. Thompson LF, et al. Crucial role for ecto-5'-nucleotidase (CD73) in vascular leakage during hypoxia. *J Exp Med.* 2004;200(11):1395-405.

27. Miska J, et al. Real-time immune cell interactions in target tissue during autoimmune-induced damage and graft tolerance. *J Exp Med.* 2014;211(3):441-56.

28. Mempel TR, et al. Regulatory T cells reversibly suppress cytotoxic T cell function independent of effector differentiation. *Immunity.* 2006;25(1):129-41.

29. Tang Q, et al. Visualizing regulatory T cell control of autoimmune responses in nonobese diabetic mice. *Nature immunology.* 2006;7(1):83-92.

30. Othy S, et al. Two-photon imaging of endogenous regulatory T cell dynamics and suppression of helper T cell priming mediated by CTLA-4. *Journal of immunology.* 2015;194.

31. Bauer CA, et al. Dynamic Treg interactions with intratumoral APCs promote local CTL dysfunction. *J Clin Invest.* 2014;124(6):2425-40.

32. Marangoni F, et al. Expansion of tumor-associated Treg cells upon disruption of a CTLA-4-dependent feedback loop. *Cell.* 2021;184(15):3998-4015 e19.

33. Darrasse-Jeze G, et al. Feedback control of regulatory T cell homeostasis by dendritic cells in vivo. *The Journal of experimental medicine.* 2009;206(9):1853-62.

34. Levine AG, et al. Continuous requirement for the TCR in regulatory T cell function. *Nature immunology.* 2014;15(11):1070-8.

35. Vahl JC, et al. Continuous T cell receptor signals maintain a functional regulatory T cell pool. *Immunity.* 2014;41(5):722-36.

36. Liu Z, et al. Immune homeostasis enforced by co-localized effector and regulatory T cells. *Nature.* 2015;528(7581):225-30.

37. Groom JR, et al. CXCR3 chemokine receptor-ligand interactions in the lymph node optimize CD4+ T helper 1 cell differentiation. *Immunity.* 2012;37(6):1091-103.

38. Di Pilato M, et al. CXCR6 positions cytotoxic T cells to receive critical survival signals in the tumor microenvironment. *Cell.* 2021;184(17):4512-30 e22.

39. Castellino F, et al. Chemokines enhance immunity by guiding naive CD8+ T cells to sites of CD4+ T cell-dendritic cell interaction. *Nature.* 2006;440(7086):890-5.

40. Coghill JM, et al. CC chemokine receptor 8 potentiates donor Treg survival and is critical for the prevention of murine graft-versus-host disease. *Blood.* 2013;122(5):825-36.

41. Rapp M, et al. CCL22 controls immunity by promoting regulatory T cell communication with dendritic cells in lymph nodes. *J Exp Med.* 2019;216(5):1170-81.

42. Akkaya B, et al. Regulatory T cells mediate specific suppression by depleting peptide-MHC class II from dendritic cells. *Nature immunology.* 2019;20(2):218-31.

43. Chaudhry A, and Rudensky AY. Control of inflammation by integration of environmental cues by regulatory T cells. *J Clin Invest.* 2013;123(3):939-44.

44. Wing K, et al. CTLA-4 control over Foxp3+ regulatory T cell function. *Science.* 2008;322(5899):271-5.

45. Kukulski F, et al. Impact of ectoenzymes on p2 and p1 receptor signaling. *Adv Pharmacol.* 2011;61:263-99.

46. Robson SC, et al. The E-NTPDase family of ectonucleotidases: Structure function relationships and pathophysiological significance. *Purinergic Signal.* 2006;2(2):409-30.

47. Kjaergaard J, et al. A2A Adenosine Receptor Gene Deletion or Synthetic A2A Antagonist Liberate Tumor-Reactive CD8(+) T Cells from Tumor-Induced Immunosuppression. *Journal of immunology.* 2018;201(2):782-91.

48. Dwyer KM, et al. Expression of CD39 by human peripheral blood CD4+ CD25+ T cells denotes a regulatory memory phenotype. *Am J Transplant.* 2010;10(11):2410-20.

49. Borsellino G, et al. Expression of ectonucleotidase CD39 by Foxp3+ Treg cells: hydrolysis of extracellular ATP and immune suppression. *Blood.* 2007;110(4):1225-32.

50. Mouri Y, et al. Lymphotoxin signal promotes thymic organogenesis by eliciting RANK expression in the embryonic thymic stroma. *Journal of immunology.* 2011;186(9):5047-57.

51. Salvalaggio PR, et al. Islet filtration: a simple and rapid new purification procedure that avoids ficoll and improves islet mass and function. *Transplantation.* 2002;74(6):877-9.

52. Liu F, and Whitton JL. Cutting edge: re-evaluating the in vivo cytokine responses of CD8+ T cells during primary and secondary viral infections. *J Immunol.* 2005;174(10):5936-40.

53. Camirand G, et al. Multiphoton intravital microscopy of the transplanted mouse kidney. *Am J Transplant.* 2011;11(10):2067-74.

54. Zhang Q, et al. CD8+ Effector T Cell Migration to Pancreatic Islet Grafts Is Dependent on Cognate Antigen Presentation by Donor Graft Cells. *Journal of immunology.* 2016;197(4):1471-6.

FIGURE LEGENDS

Figure 1. Treg can prevent allograft rejection by Teff in absence of SLO. (A) Schematic diagram of experimental design: Streptozocin-induced diabetic mice lacking SLO (splenectomized B6.LTβR$^{-/-}$; H2^{b}) were transplanted with islet allografts (Balb/c; H2^{d}). 5 days later, the mice received 2-3x10^{6} Teff or Teff + Treg from congenic wt B6 or B6.Foxp3-RFP mice (H2^{b}). **(B)** Islet allograft survival in mice lacking SLO as described in (A) that received cell transfers as indicated. Treg were from mice previously exposed to islet donor antigens (i.e. Balb/c), and naïve Treg were from naïve mice. Log-rank (Mantel-Cox) test used. **(C)** Graft-specific proliferation of Teff and Treg in absence of SLO. Representative flow cytometry histograms of CFSE dilution in transferred Teff and Treg as in (A). **(D)** Treg accumulate in allografts over time but had no effect on migration and accumulation of Teff. Left panels: Absolute cell numbers of CD4 and CD8 Teff, and of Treg within allograft over time. Right panel: Fraction of Treg within the infiltrate of transferred T cells over time. Mean +/- SEM. Multiple t tests with Holm-Sidak correction for multiple comparisons (Teff alone vs. Teff + Treg at each time point; left two panels) and Kruskal-Wallis with Dunn's multiple comparison tests (right two panels) used. **(E-F)** Treg do not affect Teff proliferation within allografts. Representative flow cytometry histograms of CFSE dilution in transferred CD8 Teff on days 3 and 5 (E). Aggregate fraction of transferred CD4 and CD8 Teff that underwent cell division on days 3 and 5 (F). Horizontal bars represent mean. Mann-Whitney tests used. N = 4-7 mice / group from at least 3 independent experiments (C-F). *: $p<0.05$. n.s.: not significant.

Figure 2. Both Teff and Treg are found in APC-rich areas surrounding transplanted islets. (A-B) Representative 3D-rendered IVM stitched-images of islet allografts and immune cells in mice lacking SLO (as in Fig. 1A) that received Teff alone (A) or Teff + Treg (B) 4 days after cells transfer. Islet surfaces were generated on fluorescently labeled transplanted islets (second column), which distinguishes between intra-islet and peri-islet cellular infiltrates (third and fourth

columns respectively). White squares demonstrate magnified areas shown at the bottom of each panel. Scale bar = 200μm (top) and 50 μm (bottom). **(C)** Treg rapidly protected transplanted islets from rejection by Teff. Violin plot of individual islet size on day 4 measured from images as in A-B. From measurements of 770-860 individual islets per group (4 mice per group). Mann-Whitney test used. **(D)** Fraction of cells within each subset that infiltrated within islets (intra-islet) from images as in A-B. **(E-F)** Intra-islet and peri-islet density of $CD11c^+$ cells (E) and T cells (F) from images as in A-B. **(G)** Fraction of Treg in the total T cell infiltrate from images as in B. Each square represents data from one mouse (D-G), and horizontal bars show median. Kruskal-Wallis with Dunn's multiple comparison tests used (D-G). *: $p<0.05$. n.s.: not significant.

Figure 3. Treg spend most of their time contacting $CD11c^+$ APCs within islet allografts. Time-lapse IVM analysis of Teff, Treg, APCs, islets, and blood vessel lumens within transplanted islets 4 days after cell transfer of Teff alone vs Teff + Treg (as in Fig. 1A). **(A)** Representative still images (left) and tracking of individual Teff and Treg (lines in right panels). Tracking lines color changes to cyan (for Teff) or to magenta (for Treg) when in contact with another cell as indicated in each panel. IVM of Teff + Treg was performed in setups where Treg were non-visible (middle panels) or visible ($eGFP^+$; bottom panels) to allow automated quantification of Teff contacts, as detailed in Materials and Methods section. **(B)** Treg increase Teff velocity. Teff and Treg velocity from movies in A. **(C)** Teff spend little time in contact with Treg, while Treg spend the majority of their time in contact with $CD11c^+$ APCs. Teff and Treg contact indexes (i.e. fraction of time spent in contact overall) with $CD11c^+$, islet, Treg and Teff cells from movies in A. Each square represents mean value from one movie, and horizontal bars show median. Mann-Whitney tests used (B-C). **(D)** Treg specifically inhibit a subpopulation of Teff that contacted both $CD11c^+$ and islet cells. ViSNE multi-parameter clustering of all Teff tracks from movies in A (left), relative value of individual parameters used in viSNE within each Teff cluster, and frequency distribution of Teff clusters (middle). Right panel depicts Teff contact index value distribution in viSNE plots. n = 3-4 mice / group using 2 or more movies for each mouse. For each movie, an average of 966 Teff

and 342 Treg were analyzed. Each square represents mean value from one movie (B-C). Horizontal bars show median. *: p<0.05. n.s.: not significant.

Figure 4. Treg preferentially contact CD11c$^+$ APCs that are substantially and simultaneously interacting with Teff. (A) Heatmap of individual CD11c$^+$ APCs and their contacts over time separated according to whether they were contacted by Teff only (left column) or by both Teff and Treg (right column; from representative Teff + Treg movie in Figure 3A). **(B-C)** Overall mean CD11c-Teff contact indexes (B), and color-coded overall mean contact indexes of CD11c$^+$ APCs (C) being contacted by Teff only or by both Teff and Treg (from Teff + Treg movies in Figure 3A). Mann-Whitney test used. n = 3-4 mice / group using 2 or more movies for each mouse. For each movie, an average of 321 CD11c+ APCs were analyzed. *: p<0.05.

Figure 5. Treg reduce expression of both MHC-II on APCs and IFN-γ in Teff within allografts. Innate immune cells were characterized by flow cytometry from islet allografts of mice lacking SLO (as described in Fig. 1A), 7 days after cell transfer. **(A)** Treg significantly reduce MHC-II, but not CD80 and CD86 expression levels on CD11c$^+$ MHC-II$^+$ innate cells within allografts. Relative mean gMFI of MHC-II, CD80 and CD86 expression levels on live CD45$^+$ Lin$^-$ CD11c$^+$ MHCII$^+$ cells within islet allografts. n=4-6 mice / group, from 2-3 independent experiments. **(B)** Treg reduce IFN-γ expression in Teff within allografts. Percentage (left) and absolute cell numbers (right) of IFNγ-expressing CD4 and CD8 Teff by direct in vivo cytokine assessment. n=5 / group, from 2 independent experiments. Each square represents data from one mouse and horizontal bars show median. Mann-Whitney tests used. *: p <0.05. n.s.: not significant.

Figure 6. Treg suppressor function within allografts is dependent on the ecto-nucleotidase CD73. (A) Wt and CD73$^{-/-}$ Treg display equal suppressive capacity *in vitro*. Proliferation results from in vitro suppression assays. From 2 experiments. Kruskal-Wallis tests used. **(B)** Unlike wt Treg, CD73$^{-/-}$ Treg fail to protect from rejection within allografts. Graft survival in mice lacking SLO

bearing islet allografts (as described in Fig. 1A) received cells as indicated. Graft survival data in Teff and Teff + wt Treg groups are from Fig. 1B. Log-rank (Mantel-Cox) tests used. **(C)** Time-lapse IVM of Teff + CD73$^{-/-}$ Treg within transplanted islets 4 days after cell transfer. Representative still images (left) and tracking of individual Teff and Treg (lines in right panels). Tracking lines color changes to cyan (for Teff) or to magenta (for Treg) when in contact with other cells as indicated in each panel. IVM of Teff + CD73$^{-/-}$ Treg was performed in setups where Treg were non-visible (top panel) or visible (GFP; bottom panel) to allow automated quantification of Teff contacts, as detailed in Material and Method section. **(D)** Teff and Treg velocity from movies in C (Teff + CD73$^{-/-}$ Treg) and Fig. 3A (Teff + wt Treg). Teff + wt Treg data are from Fig. 3B. **(E)** CD73$^{-/-}$ Treg contacted CD11c^{+} APCs significantly less than wt Treg. Teff, wt Treg and CD73$^{-/-}$ Treg contact indexes from movies as in D. Teff + wt Treg data are from Fig. 3C. Mann-Whitney tests used (D-E). **(F)** The behavior of wt Treg and CD73$^{-/-}$ Treg within allografts further differs at sub-population levels. ViSNE multi-parameter clustering of all Treg tracks from movies in A and in Fig. 3A (left), relative value of individual parameters used in viSNE within each Treg cluster (middle) and frequency distribution of Treg clusters (right). Bottom left panel depicts Treg contact index value distribution in viSNE plots. n = 3 mice / group using 2 or more movies for each mouse. For each movie, an average of 1120 Teff and 500 Treg were analyzed. Each square represents mean value from one movie (D-E). Horizontal bars show median. *: $p < 0.05$. n.s.: not significant.

SUPPLEMENTAL MATERIAL

Supplemental Figure 1 (Complement to Fig. 1). Treg can prevent allograft rejection by Teff in a second SLO-deficient mouse model (splenectomized *aly/aly* recipients), and freshly activated Treg provide complete protection from rejection. (A-B) Islet allograft survival in splenectomized *aly/aly* recipients that received cell transfers as indicated and as described in Fig. 1A. Treg were from mice previously exposed to donor antigens, while "naïve Treg" were from naïve mice. Log-rank (Mantel-Cox) test used. **(C)** We tested whether freshly activated Treg would provide better protection from rejection in our model. Islet allograft survival in splenectomized LTβR$^{-/-}$ recipients that received 2-3x10^6 CD44^{Hi} sorted Teff alone, or with 2-3x10^6 Treg from freshly immunized mice against donor antigens. Using freshly activated Treg provided protection from rejection in 100% of the recipients. This approach was then used for our IVM studies.

Supplemental Figure 2 (Complement to Fig. 3 and Fig. 6). Treg contacts with CD11c$^+$ APCs are longer and more frequent than those with Teff, and this is lost when Treg lack CD73 expression. (A) Treg contact CD11c$^+$ APCs more than Teff. Teff and Treg contact time (left) and contact frequency (right) with CD11c$^+$ APCs, islet, Treg and Teff cells from movies in Fig. 3A. **(B)** CD73$^{-/-}$ Treg, which cannot suppress within allografts, demonstrate reduced interactions with CD11c$^+$ APCs compared to wt Treg. Teff and Treg contact time (left) and contact frequency (right) with CD11c$^+$ APCs, islet, Treg and Teff cells from movies in Fig. 6C. Each square represents mean value from one movie and horizontal bars show medians. n = 3-4 mice / group using 2 or more movies for each mouse (A-B). **(C)** CD73$^{-/-}$ Treg exhibit similar dynamics than wt Treg in steady state. IVM of CD73$^{-/-}$ Treg and wt Treg in spleen of naïve B6.CD11c-YFP mice 2 days after cell transfer. Speed and Treg-CD11c$^+$ APC contact indexes of wt and CD73$^{-/-}$ Treg. Each square represents mean value from one movie and horizontal bars show medians. N = 2 mice / group, from 2 independent experiments. 2 movies / mouse were analyzed. Mann-Whitney tests used (A-C). *: $p < 0.05$. n.s.: not significant.

Supplemental Figure 3 (Complement to Fig. 5). Treg did not substantially affect the phenotype of innate immune cells infiltrating allografts. Innate immune cells were characterized by flow cytometry from islet allografts of mice lacking SLO (as described in Fig. 1A), 7 days after cell transfer. **(A)** Nearly all innate immune cells within islet allografts expressed CD11c (Left panel; gated on live $CD45^+$ Lin^- $NK1.1^-$ $Ly6G^-$). $CD11c^+$ cells were clustered with ViSNE using the markers listed in B. tSNE plots and relative expression levels of selected markers shown (right). **(B)** ViSNE cluster analysis demonstrates that Treg induce a slight decrease in frequency of clusters 5 and 6, which express MHC-II and some CD80 and CD86, and a correlate slight increase in frequency of clusters expressing low levels of MHC-II, CD80 and CD86. Left: representative ViSNE plots and clustering for each group. Right: Heat map of relative expression of various markers within individual clusters, and frequency of each cluster within the entire $CD11c^+$ cell population. Representative of 2 independent experiments, n=2 mice / group / experiment.

Supplemental Movie 1 (Complement to Fig. 3). Time-lapse IVM of islet allograft rejection by Teff. Representative time-lapse IVM of transplanted allogenic islet rejection by Teff on day 4. Splenectomized B6.LTβ$R^{-/-}$ mice reconstituted with bone marrow from B6.CD11c-YFP were transplanted with CTO-stained Balb/c islets under the kidney capsule and received Teff isolated from B6.CFP mice. Blood vessel lumens were identified using Evans blue. The first segment of the movie demonstrates blood flow and blood vessels within the imaging volume. The second segment show Teff dynamics (same movie played twice). The third segment show various perspectives of all Teff tracks (red lines), $CD11c^+$ APCs (blue surfaces), and transplanted islets (cyan surfaces) within the imaging volume.

Supplemental Movie 2 (Complement to Fig. 3). Dynamics of Teff making prolonged contacts with transplanted islets during rejection. Representative time-lapse IVM of Teff

crawling on the surface and through transplanted allogeneic islets during rejection (as described in supplemental movie 1). The first segment of the movie demonstrates Teff crawling on the surface of transplanted islets. The second and third movie segments show examples of Teff crawling through transplanted islets. Teff tracking lines change color from red to cyan when Teff are contacting islets.

Supplemental Movie 3 (Complement to Fig. 3). Time-lapse IVM of Treg suppression of islet allograft rejection. Representative time-lapse IVM of Treg suppression of transplanted allogenic islet rejection by Teff on day 4. Experimental approach as in Supplemental Movie 1, except that the mice received Treg from Foxp3-RFP.CD90.1.eGFP mice concomitantly with Teff. The first segment of the movie demonstrates blood flow and blood vessels within the imaging volume. The second segment show Teff and Treg dynamics (same movie played twice). The third segment shows various perspectives of all Teff and Treg tracks (red and green lines respectively), $CD11c^+$ APCs (blue surfaces), and transplanted islets (cyan surfaces) within the imaging volume.

Supplemental Movie 4 (Complement to Fig. 3). Example of Treg-APC continuous interactions while the same APC simultaneously interacts with Teff. Time-lapse IVM of Treg-APC-Teff interactions using software-generated surfaces. Experimental approach as in Supplemental Movie 3. Top panel showing Treg and APC only, and bottom panel showing Teff, Treg and APC from the same movie.

Figure 1

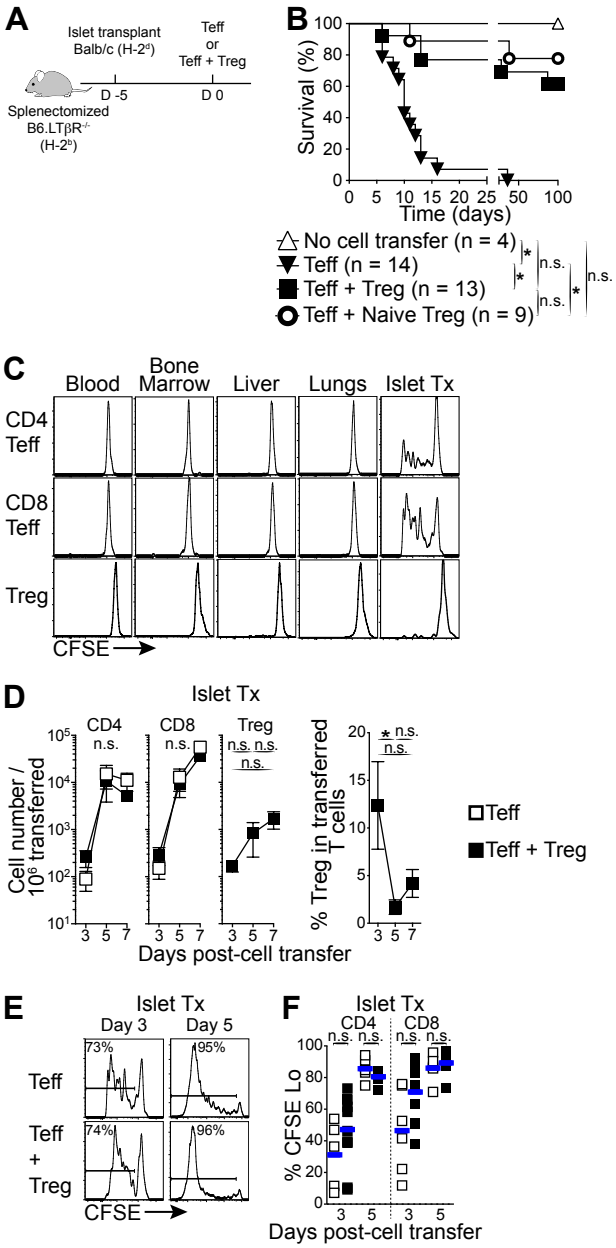

Figure 1. Treg can prevent allograft rejection by Teff in absence of SLO. (A) Schematic diagram of experimental design: Streptozocin-induced diabetic mice lacking SLO (splenectomized B6.LTβR$^{-/-}$; H2b) were transplanted with islet allografts (Balb/c; H2^{d}). 5 days later, the mice received 2-3x10^{6} Teff or Teff + Treg from congenic wt B6 or B6.Foxp3-RFP mice (H2^{b}). **(B)** Islet allograft survival in mice lacking SLO as described in (A) that received cell transfers as indicated. Treg were from mice previously exposed to islet donor antigens (i.e. Balb/c), and naïve Treg were from naïve mice. Log-rank (Mantel-Cox) test used. **(C)** Graft-specific proliferation of Teff and Treg in absence of SLO. Representative flow cytometry histograms of CFSE dilution in transferred Teff and Treg as in (A). **(D)** Treg accumulate in allografts over time but had no effect on migration and accumulation of Teff. Left panels: Absolute cell numbers of CD4 and CD8 Teff, and of Treg within allograft over time. Right panel: Fraction of Treg within the infiltrate of transferred T cells over time. Mean +/- SEM. Multiple t tests with Holm-Sidak correction for multiple comparisons (Teff alone vs. Teff + Treg at each time point; left two panels) and Kruskal-Wallis with Dunn's multiple comparison tests (right two panels) used. **(E-F)** Treg do not affect Teff proliferation within allografts. Representative flow cytometry histograms of CFSE dilution in transferred CD8 Teff on days 3 and 5 (E). Aggregate fraction of transferred CD4 and CD8 Teff that underwent cell division on days 3 and 5 (F). Horizontal bars represent mean. Mann-Whitney tests used. N = 4-7 mice / group from at least 3 independent experiments (C-F). *: p<0.05. n.s.: not significant.

Figure 2

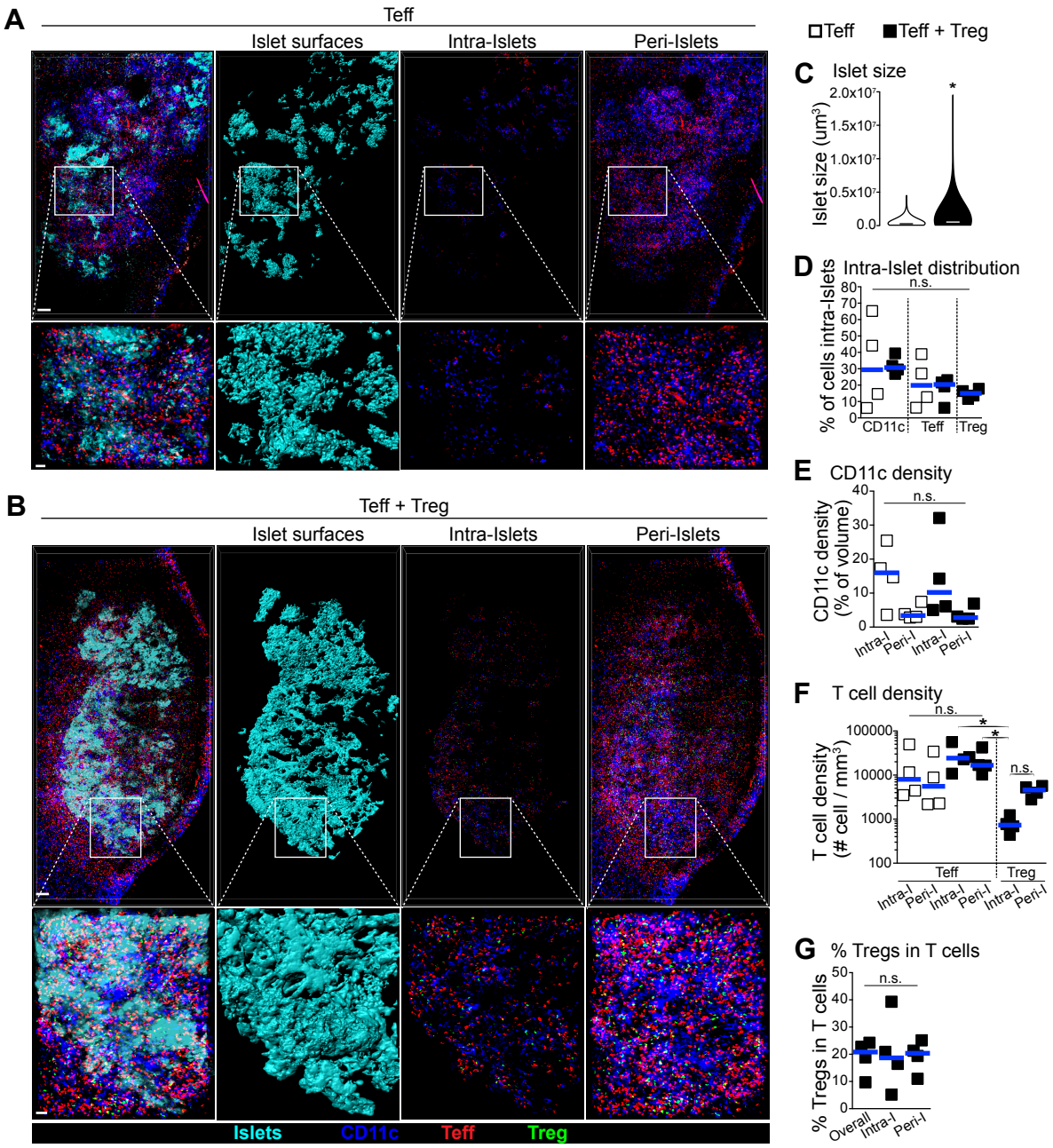

Figure 2. Both Teff and Treg are found in APC-rich areas surrounding transplanted islets. (A-B) Representative 3D-rendered IVM stitched-images of islet allografts and immune cells in mice lacking SLO (as in Fig. 1A) that received Teff alone (A) or Teff + Treg (B) 4 days after cells transfer. Islet surfaces were generated on fluorescently labeled transplanted islets (second column), which distinguishes between intra-islet and peri-islet cellular infiltrates (third and fourth columns respectively). White squares demonstrate magnified areas shown at the bottom of each panel. Scale bar = 200μm (top) and 50μm (bottom). **(C)** Treg rapidly protected transplanted islets from rejection by Teff. Violin plot of individual islet size on day 4 measured from images as in A-B. From measurements of 770-860 individual islets per group (4 mice per group). Mann-Whitney test used. **(D)** Fraction of cells within each subset that infiltrated within islets (intra-islet) from images as in A-B. **(E-F)** Intra-islet and peri-islet density of CD11c cells (E) and T cells (F) from images as in A-B. **(G)** Fraction of Treg in the total T cell infiltrate from images as in B. Each square represents data from one mouse (D-G), and horizontal bars show median. Kruskal-Wallis with Dunn's multiple comparison tests used (D-G). *: $p<0.05$. n.s.: not significant.

Figure 3

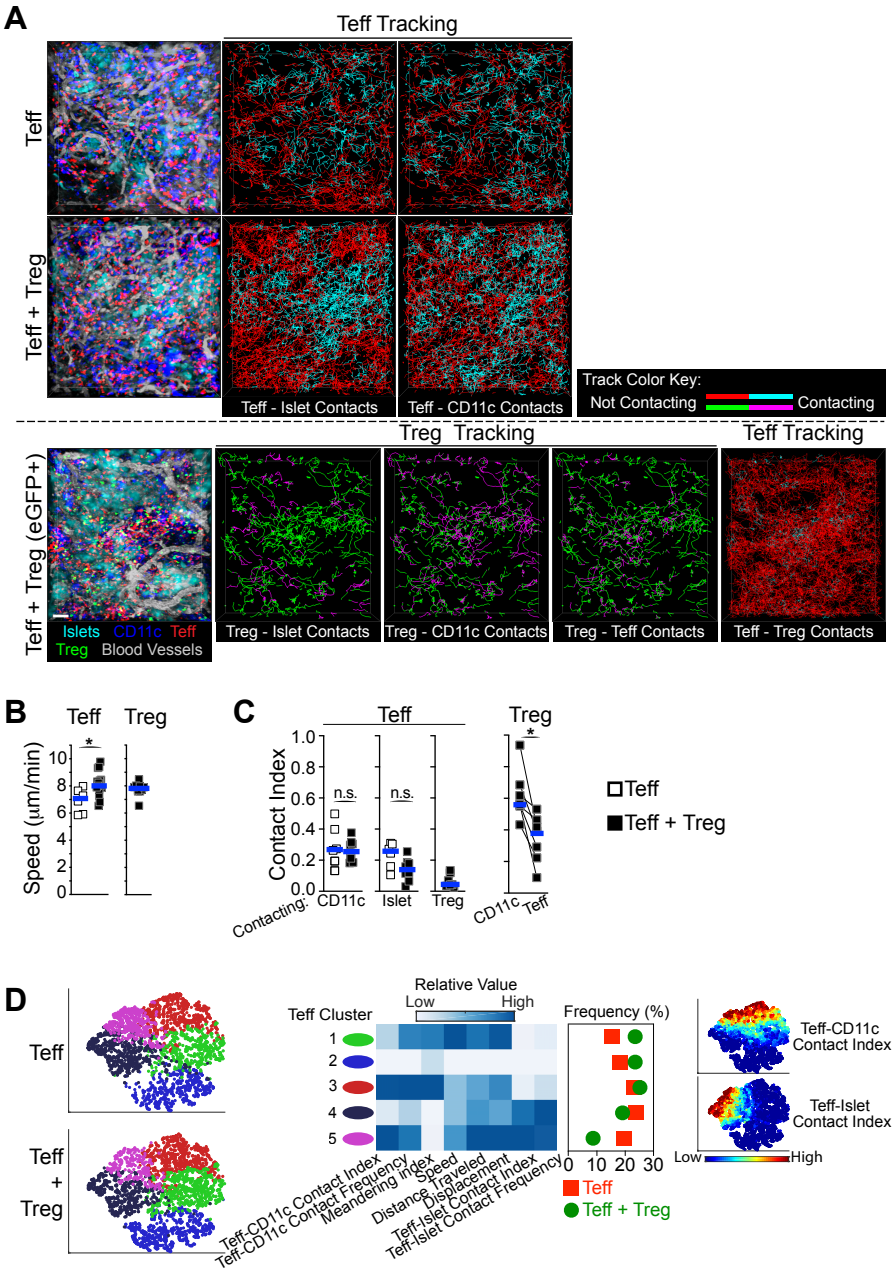

Figure 3. Treg spend most of their time contacting CD11c+ APCs within islet allografts. Time-lapse IVM analysis of Teff, Treg, APCs, islets, and blood vessel lumens within transplanted islets 4 days after cell transfer of Teff alone vs Teff + Treg (as in Fig. 1A). **(A)** Representative still images (left) and tracking of individual Teff and Treg (lines in right panels). Tracking lines color changes to cyan (for Teff) or to magenta (for Treg) when in contact with another cell as indicated in each panel. IVM of Teff + Treg was performed in setups where Treg were non-visible (middle panels) or visible (eGFP$^+$; bottom panels) to allow automated quantification of Teff contacts, as detailed in Materials and Methods section. **(B)** Treg increase Teff velocity. Teff and Treg velocity from movies in A. **(C)** Teff spend little time in contact with Treg, while Treg spend the majority of their time in contact with CD11c$^+$ APCs. Teff and Treg contact indexes (i.e. fraction of time spent in contact overall) with CD11c$^+$, islet, Treg and Teff cells from movies in A. Each square represents mean value from one movie, and horizontal bars show median. Mann-Whitney tests used (B-C). **(D)** Treg specifically inhibit a subpopulation of Teff that contacted both CD11c$^+$ and islet cells. ViSNE multi-parameter clustering of all Teff tracks from movies in A (left), relative value of individual parameters used in viSNE within each Teff cluster, and frequency distribution of Teff clusters (middle). Right panel depicts Teff contact index value distribution in viSNE plots. n = 3-4 mice / group using 2 or more movies for each mouse. For each movie, an average of 966 Teff and 342 Treg were analyzed. Each square represents mean value from one movie (B-C). Horizontal bars show median. *: $p<0.05$. n.s.: not significant.

Figure 4

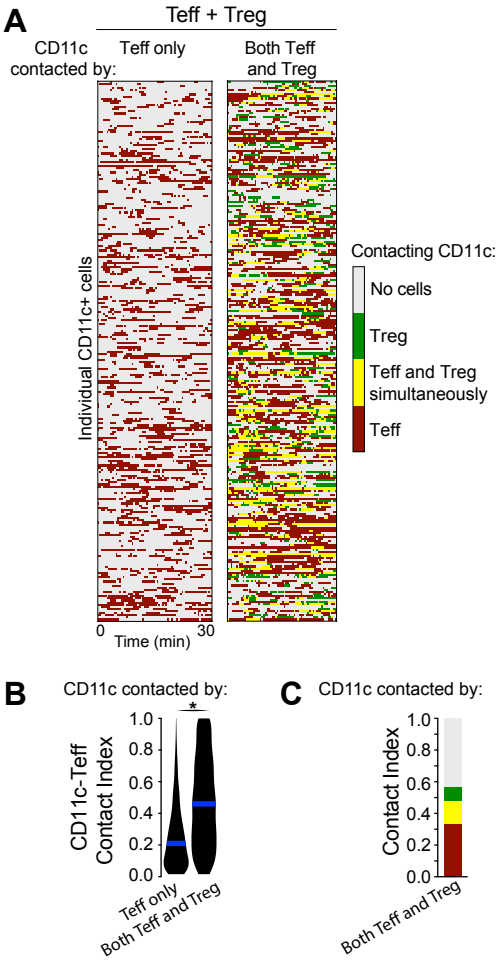

Figure 4. Treg preferentially contact CD11c⁺ APCs that are substantially and simultaneously interacting with Teff. **(A)** Heatmap of individual CD11c⁺ APCs and their contacts over time separated according to whether they were contacted by Teff only (left column) or by both Teff and Treg (right column; from representative Teff + Treg movie in Figure 3A). **(B-C)** Overall mean CD11c-Teff contact indexes (B), and color-coded overall mean contact indexes of CD11c⁺ APCs (C) being contacted by Teff only or by both Teff and Treg (from Teff + Treg movies in Figure 3A). Mann-Whitney tests used. n = 3-4 mice / group using 2 or more movies for each mouse. For each movie, an average of 321 CD11c+ APCs were analyzed. *: $p<0.05$.

Figure 5

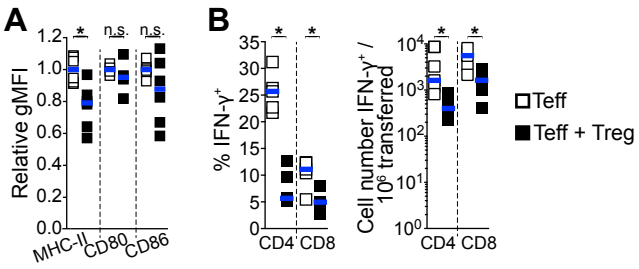

Figure 5. Treg reduce expression of both MHC-II on APCs and IFN-γ in Teff within allografts. Innate immune cells were characterized by flow cytometry from islet allografts of mice lacking SLO (as described in Fig. 1A), 7 days after cell transfer. **(A)** Treg significantly reduce MHC-II, but not CD80 and CD86 expression levels on $CD11c^+$ $MHC\text{-}II^+$ innate cells within allografts. Relative mean gMFI of MHC-II, CD80 and CD86 expression levels on live $CD45^+$ Lin^- $CD11c^+$ $MHCII^+$ cells within islet allografts. n=4-6 mice / group, from 2-3 independent experiments. **(B)** Treg reduce IFN-γ expression in Teff within allografts. Percentage (left) and absolute cell numbers (right) of IFNγ-expressing CD4 and CD8 Teff by direct in vivo cytokine assessment. n=5 / group, from 2 independent experiments. Each square represents data from one mouse and horizontal bars show median. Mann-Whitney tests used. *: $p < 0.05$. n.s.: not significant.

Figure 6

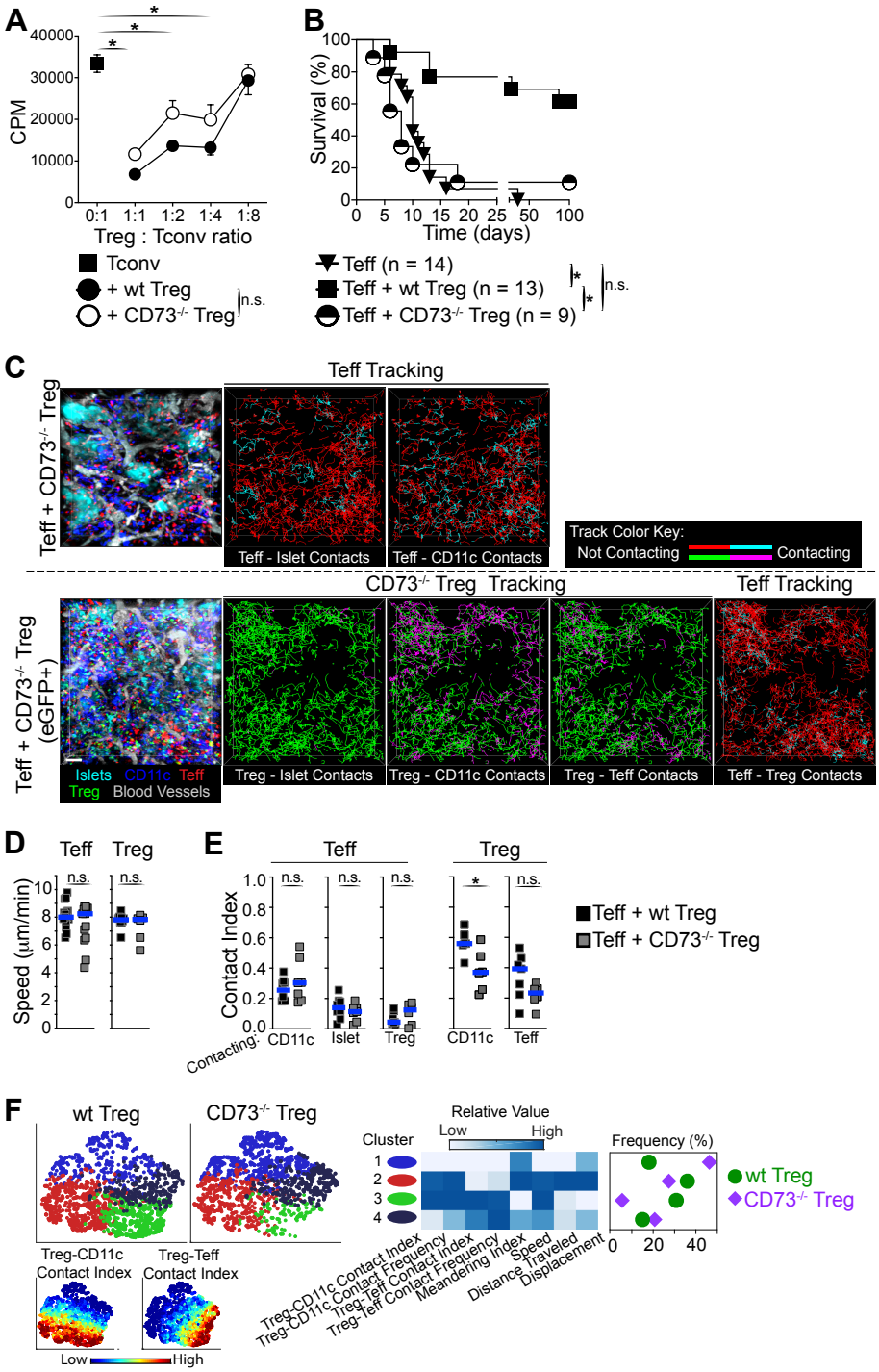

Figure 6. Treg suppressor function within allografts is dependent on the ecto-nucleotidase CD73. (A) Wt and CD73$^{-/-}$ Treg display equal suppressive capacity in vitro. Proliferation results from in vitro suppression assays. From 2 experiments. Kruskal-Wallis tests used. **(B)** Unlike wt Treg, CD73**-/-** Treg fail to protect from rejection within allografts. Graft survival in mice lacking SLO bearing islet allografts (as described in Fig. 1A) received cells as indicated. Graft survival data in Teff and Teff + wt Treg groups are from Fig. 1B. Log-rank (Mantel-Cox) tests used. **(C)** Time-lapse IVM of Teff + CD73$^{-/-}$ Treg within transplanted islets 4 days after cell transfer. Representative still images (left) and tracking of individual Teff and Treg (lines in right panels). Tracking lines color changes to cyan (for Teff) or to magenta (for Treg) when in contact with other cells as indicated in each panel. IVM of Teff + CD73$^{-/-}$ Treg was performed in setups where Treg were non-visible (top panel) or visible (GFP; bottom panel) to allow automated quantification of Teff contacts, as detailed in Material and Method section. **(D)** Teff and Treg velocity from movies in C (Teff + CD73$^{-/-}$ Treg) and Fig. 3A (Teff + wt Treg). Teff + wt Treg data are from Fig. 3B. **(E)** CD73$^{-/-}$ Treg contacted CD11c^{+} APCs significantly less than wt Treg. Teff, wt Treg and CD73$^{-/-}$ Treg contact indexes from movies as in D. Teff + wt Treg data are from Fig. 3C. Mann-Whitney tests used (D-E). **(F)** The behavior of wt Treg and CD73$^{-/-}$ Treg within allografts further differs at sub-population levels. ViSNE multi-parameter clustering of all Treg tracks from movies in A and in Fig. 3A (left), relative value of individual parameters used in viSNE within each Treg cluster (middle) and frequency distribution of Treg clusters (right). Bottom left panel depicts Treg contact index value distribution in viSNE plots. n = 3 mice / group using 2 or more movies for each mouse. For each movie, an average of 1120 Teff and 500 Treg were analyzed. Each square represents mean value from one movie (D-E). Horizontal bars show median. *: p <0.05. n.s.: not significant.

Supplemental Figure 1

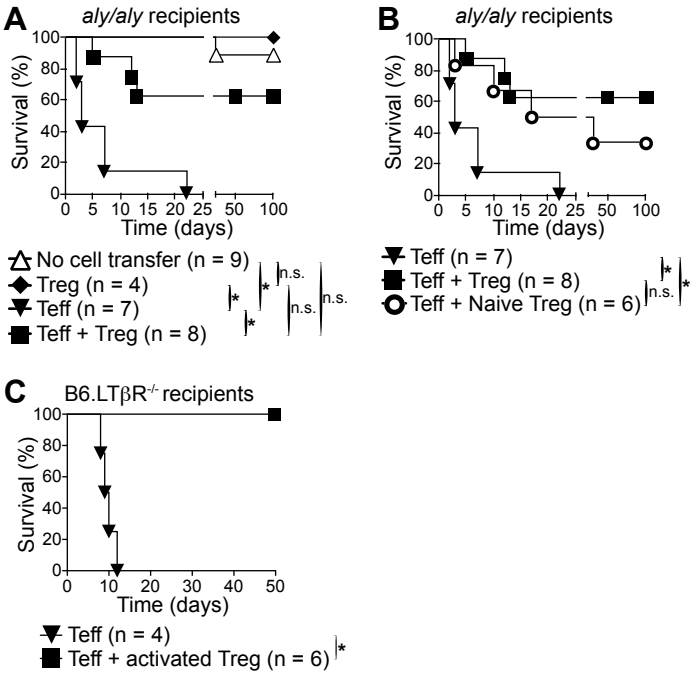

Supplemental Figure 1 (Complement to Fig. 1). Treg can prevent allograft rejection by Teff in a second SLO-deficient mouse model (splenectomized aly/aly recipients), and freshly activated Treg provide complete protection from rejection.

(A-B) Islet allograft survival in splenectomized aly/aly recipients that received cell transfers as indicated and as described in Fig. 1A. Treg were from mice previously exposed to donor antigens, while “naïve Treg” were from naïve mice. Log-rank (Mantel-Cox) test used.

(C) We tested whether freshly activated Treg would provide better protection from rejection in our model. Islet allograft survival in splenectomized LTβR-/- recipients that received 2-3x10^6 CD44Hi sorted Teff alone, or with 2-3x10^6 Treg from freshly immunized mice against donor antigens. Using freshly activated Treg provided protection from rejection in 100% of the recipients. This approach was then used for our IVM studies.

Supplemental Figure 2

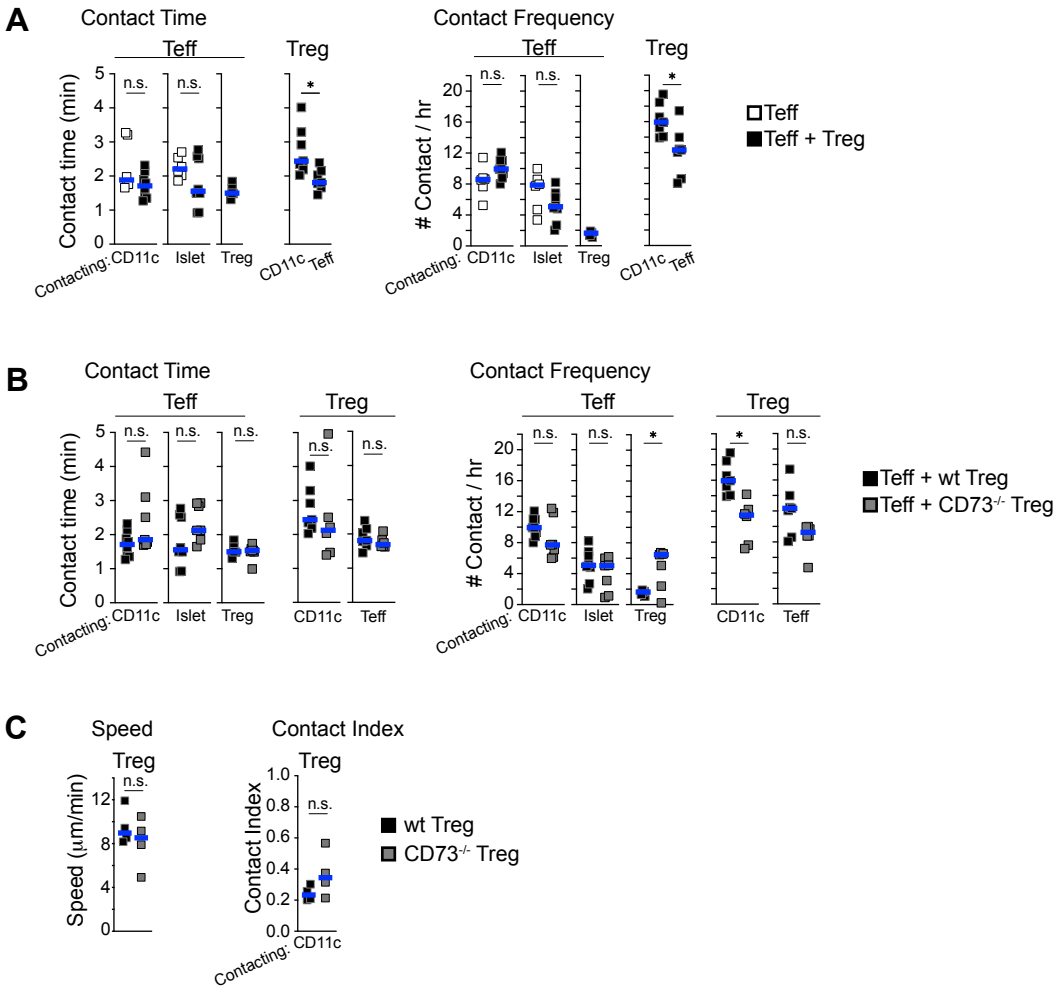

Supplemental Figure 2 (Complement to Fig. 3 and Fig. 6). Treg contacts with CD11c⁺ APCs are longer and more frequent than those with Teff, and this is lost when Treg lack CD73 expression.
(A) Treg contact CD11c⁺ APCs more than Teff. Teff and Treg contact time (left) and contact frequency (right) with CD11c+ APCs, islet, Treg and Teff cells from movies in Fig. 3A.
(B) CD73$^{-/-}$ Treg, which cannot suppress within allografts, demonstrate reduced interactions with CD11c⁺ APCs compared to wt Treg. Teff and Treg contact time (left) and contact frequency (right) with CD11c⁺ APCs, islet, Treg and Teff cells from movies in Fig. 6C. Each square represents mean value from one movie and horizontal bars show medians. N = 3-4 mice / group using 2 or more movies for each mouse (A-B).
(C) CD73$^{-/-}$ Treg exhibit similar dynamics than wt Treg in steady state. IVM of CD73$^{-/-}$ Treg and wt Treg in spleen of naïve B6.CD11c-YFP mice 2 days after cell transfer. Speed and Treg-CD11c⁺ APC contact indexes of wt and CD73$^{-/-}$ Treg. Each square represents mean value from one movie and horizontal bars show medians. N = 2 mice / group, from 2 independent experiments. 2 movies / mouse were analyzed. Mann-Whitney tests used (A-C). *: p <0.05. n.s.: not significant.

Supplemental Figure 3

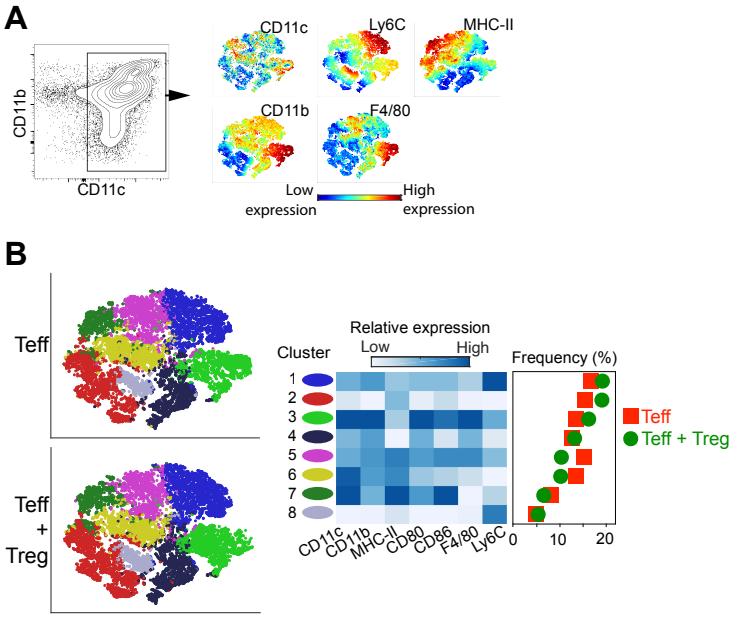

Supplemental Figure 3 (Complement to Fig. 5). Treg did not substantially affect the phenotype of innate immune cells infiltrating allografts. Innate immune cells were characterized by flow cytometry from islet allografts of mice lacking SLO (as described in Fig. 1A), 7 days after cell transfer.
(A) Nearly all innate immune cells within islet allografts expressed CD11c (Left panel; gated on live CD45+ Lin- NK1.1- Ly6G-). CD11c+ cells were clustered with ViSNE using the markers listed in B. tSNE plots and relative expression levels of selected markers shown (right).
(B) ViSNE cluster analysis demonstrates that Treg induce a slight decrease in frequency of clusters 5 and 6, which express MHC-II and some CD80 and CD86, and a correlate slight increase in frequency of clusters expressing low levels of MHC-II, CD80 and CD86. Left: representative ViSNE plots and clustering for each group. Right: Heat map of relative expression of various markers within individual clusters, and frequency of each cluster within the entire CD11c+ cell population. Representative of 2 independent experiments, n=2 mice / group / experiment.